Journal of Engineering and Sustainable Development
Vol. 28, No. 04, September 2024
https://jeasd.uomustansiriyah.edu.iq/index.php/jeasd
ISSN 2520-0917
Research Article
https://doi.org/10.31272/jeasd.28.5.10

Improvement Underwater Acoustic Signal De-Noising Based on Dual-Tree Complex Wavelet Transform

Ausama Khalid[1*], Yasin Al-Aboosi[2], Nor Shahida Mohd Shah[3]

[1,2]Electrical Engineering Department, College of Engineering, Mustansiriyah University, Baghdad, Iraq
[3]Faculty of Engineering, University Tun Hussein Onn Malaysia, Parity Raja, Malaysia

[1]https://orcid.org/0000-0002-5456-3533
[2]https://orcid.org/0000-0002-9918-7770
[3]https://orcid.org/0000-0001-8759-0426
[*]Email: asamaw.khalid@uomustansiriyah.edu.iq

Article Info

Received	13/04/2023
Revised	15/08/2024
Accepted	19/08/2024

Abstract

Underwater Acoustic signal denoising is encountering high demand due to the extensive use of acoustic in a lot of underwater applications. Underwater acoustic noise (UWAN) has a high effect on the quality of the acoustic signal therefore, it is always preferred to use a de-noising filter to remove it. In this paper, we propose a filter that utilizes a Complex wavelet transform (CWT) to remove UWAN and help improve the signal-to-noise ratio (SNR) of the detected acoustic signal. CWT is nearly shift-invariant and offers a good directionality in contrast to normal wavelet transform (DWT). The proposed method was tested using a real recorded UWAN for three depths from the Tigris River. The proposed method was compared with a more conveniently used discrete wavelet transform. The test included using Two signals: fixed frequency and linear modulation signal. De-noising was performed using a soft thresholding technique based on level-dependent threshold estimation. The proposed method showed supreme performance in terms of SNR and root mean square error (RMSE). When the input signal was 5.9 dB and -13.2 dB for SNR and RMSE respectively, the results were 10.9 dB for SNR and -15.7 dB for RMSE in the case of fixed frequency.

Keywords: Acoustic noise; Complex wavelet transform; Signal de-noising; Wavelet transform.

1. Introduction

The need for underwater channels of communication has experienced significant growth as a result of many activities, including pollution monitoring, offshore oil prospecting, and military operations involving submarine communication [1]. Electromagnetic waves are not dependable for transmitting information over long distances because the waves experience significant attenuation, which weakens the waves [1]-[3]. Therefore, electromagnetic waves are suitable for relatively small distances, namely up to 10 meters [4]. Alternatively, acoustical waves are commonly used for underwater communication since such waves are less likely to be attenuated [1], [2]. Acoustic waves are subject to significant issues, one of which is underwater acoustic noise (UWAN). This issue mostly affects the quality of the signal. Underwater acoustic noise (UWAN) can originate from either human activities (such as ships, pumps, and power plants) or natural sources (such as snapping shrimp, wind, and currents) [5]. The existence of UWAN leads to a rise in the bit error rate, resulting in a decrease in the overall system performance. Therefore, using a de-noising approach is crucial to restoring the original signal.

Since signal de-noising helps restore the original signal, especially when distorted by noise, de-noising is a crucial issue for many applications. The majority of de-noising techniques treat noise as Additive White Gaussian Noise (AWGN), where the strength of the noise is evenly distributed across all frequency ranges [6]. For this, several methods and algorithms are employed, including the Wiener filter [7], median and mean filters [8], singular value decomposition [9], and others. Although the Wiener filter is employed When the signal-to-noise ratio (SNR) is reasonably high, the Wiener filter can lead to speech distortion during the process of removing noise [7]. Currently, the most often employed and effective method for reducing noise in a signal is the use of wavelet transform (WT). Many approaches, including wavelet shrinkage [10] and wavelet correlation [11], have been suggested based on the WT approach, and have demonstrated good performance in de-noising signals. WT-based de-noising approaches include

applying nonlinear operations to signal coefficients obtained after the transformation and then reconstructing the signal using the modified coefficients. Among these techniques, wavelet thresholding is the recommended way for reducing noise because the wavelet can effectively enhance the SNR and has a comparatively low root mean square error (RMSE) [11], [12]. Typically, previous techniques treat the noise as an AWGN [9], [10]. However, some studies have defined UWAN as non-Gaussian and colored noise such as [13]-[15], and [16]. To solve this issue, two methods are under consideration: the first method includes implementing the pre-whitening stage before the wavelet de-noising stage, and then treating the generated data as white noise throughout processing [6]. As an alternative to the pre-whitening stage, suitable level-dependent thresholding is implemented in the second method.

This work utilizes a de-noising filter, namely the Dual-Tree complex Discrete Wavelet Transform (DT-DWT) based on Selesnick's work [17], to process acoustic signals in the existence of UWAN [18]. DT-DWT is commonly known as the complex wavelet transform (CWT), since CWT is derived from two trees, one representing the real part and the other representing the imaginary part. DT-DWT serves as a replacement for wavelet decomposition [11]. DT-DWT has demonstrated higher performance compared to regular DWT in terms of SNR and RMSE values by utilizing level-dependent thresholding.

The paper is structured in the following manner. Section 2 presents an analysis of UWAN noise and defines the signals employed. Section 3 details the execution of discrete wavelet transform (DWT) and the proposed complex wavelet transform de-noising techniques. The discussion of the results is included in Section 4. Lastly, our conclusions are presented in Section 5.

2. Acoustic Signal and Noise

Noise is a major issue in various communication channels, motivating several efforts to limit or wipe out its impact on signals, as demonstrated by previous studies [7]-[9], [11]. This part will focus on the signal utilized in the simulation and analyze UWAN, a colored signal, for de-noising in a presumed additive channel.

2.1. Signal Model

The signals employed consist of sinusoidal waves, namely linear frequency modulation (LFM) to depict a signal that changes over time, and a constant-frequency wave to indicate a constant frequency. Practically, a sinusoidal signal may be mathematically represented as:

$$S(n) = \begin{cases} A\sin\big(\theta(n)\big) & 0 < n \leq N-1 \\ 0 & \text{otherwise} \end{cases} \quad (1)$$

The signal's instantaneous phase is denoted by $\theta(n)$, and N is the number of samples in the signal. It's possible to express the instantaneous phase for a given frequency as:

$$\theta(n) = 2\pi f_m \, n \, T_s \quad (2)$$

Where T_s is the sampling time and f_m is the signal frequency. The definition of $\theta(n)$ for the LFM signal is as follows:

$$\theta(n) = 2\pi \left(f_m + \frac{\varphi}{2} n \, T_s\right) n \, T_s \quad (3)$$

Where the signal bandwidth is represented by f_{BW}, and the frequency, represented by φ, is specified by $\varphi = \frac{f_{BW}}{NT_s}$.

The definition of the detected signal is as follows:

$$x(n) = s(n) + v(n) \quad (4)$$

Where $v(n)$ denotes the UWAN and $s(n)$ is the intended signal.

2.2. Characteristics of UWAN.

UWAN has non-Gaussian characteristics, particularly in shallow water, due to the presence of impulsive behavior of snapping-shrimp noise [14], [16]. The power spectral density (PSD) decreases with frequency increase and is defined as colored noise. PSD is dependent on the frequency [13]. Hence, the Power Spectral Density (PSD) of UWAN may be accurately characterized as:

$$S_x(e^{i\omega}) = \frac{1}{f^B} \qquad where\ B > 0 \quad (5)$$

Field tests and useful measurements have been used to examine the properties of UWAN [16]. Previous studies, including [13]-[19], have discovered that UWAN matches the student's t-distribution, a statistical distribution with a defined shape factor or degree of freedom. UWAN has the noise source's effect on its degree of freedom varies between environments, from shallow water to deep water [1]. For a student's t-distribution, a density of probability (PDF) is given as follows [18]:

$$\rho(y, v) = \frac{\Gamma\left(\frac{1+v}{2}\right)}{\sqrt{\pi x}\Gamma\left(\frac{v}{2}\right)}\left(1 + \frac{y^2}{v}\right)^{\frac{-(1+v)}{2}} \quad (6)$$

The symbol $\Gamma(.)$ denotes the function of gamma, whereas v indicates a degree or level of freedom. The PDF shown in (6) has a mean of zero and a variance equivalent to v/(v-2) for v greater than or equal to 2. The Function of PDF of different degrees of freedom is shown in Fig. 1, Student's t-distributions converge to a normal distribution as v approaches infinity [13].

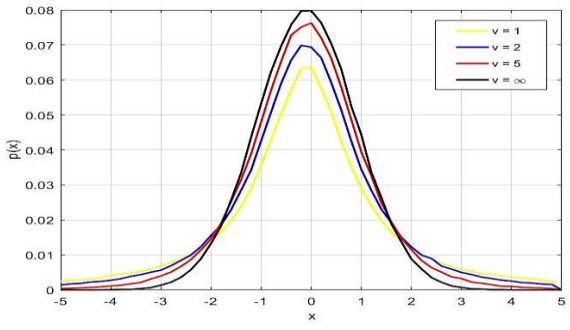

Figure 1. The student t-distribution PDF for different levels of freedom v [13].

In Fig. 2, which displays a time model of three depths and an autocorrelation function (ACF) generated for each depth, real data taken straight from a river is shown. The samples were collected by Mahmood in the Tigris River [19]. The noise signal is determined using a sampling frequency of 8000 Hz. As seen in Fig 2, the autocorrelation function (ACF) does not exhibit a delta Dirac function δ(n), indicating that the UWAN seems to be colored noise [6]. After evaluating the samples taken from the river, v = 2.5 was found to be the degree of freedom [14], [19]. The pdf function may be expressed as follows:

$$\rho(y, 2.5) = 0.5721\left(\frac{y^2}{2.5} + 1\right)^{-1.75} \quad (7)$$

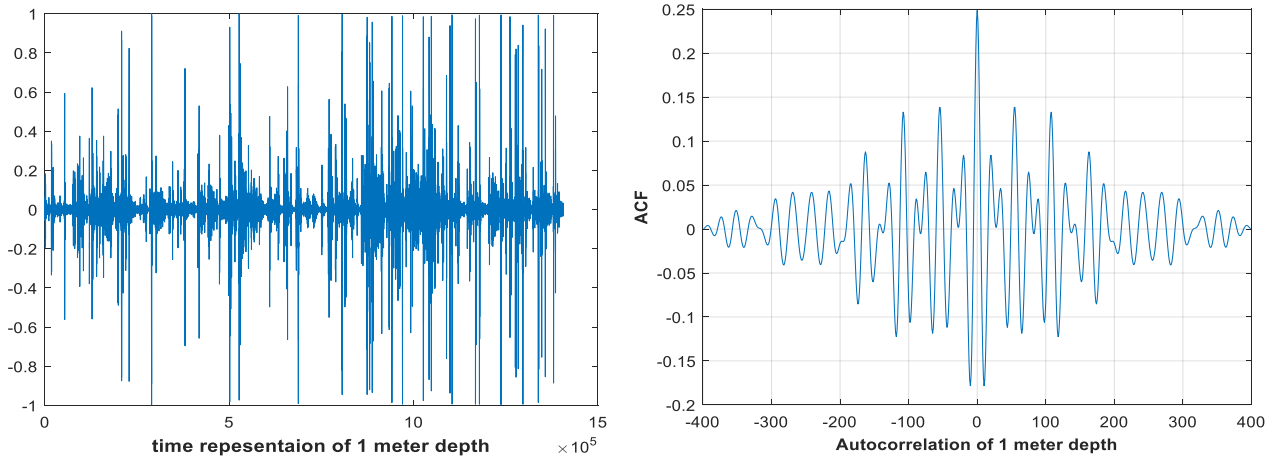

(a)

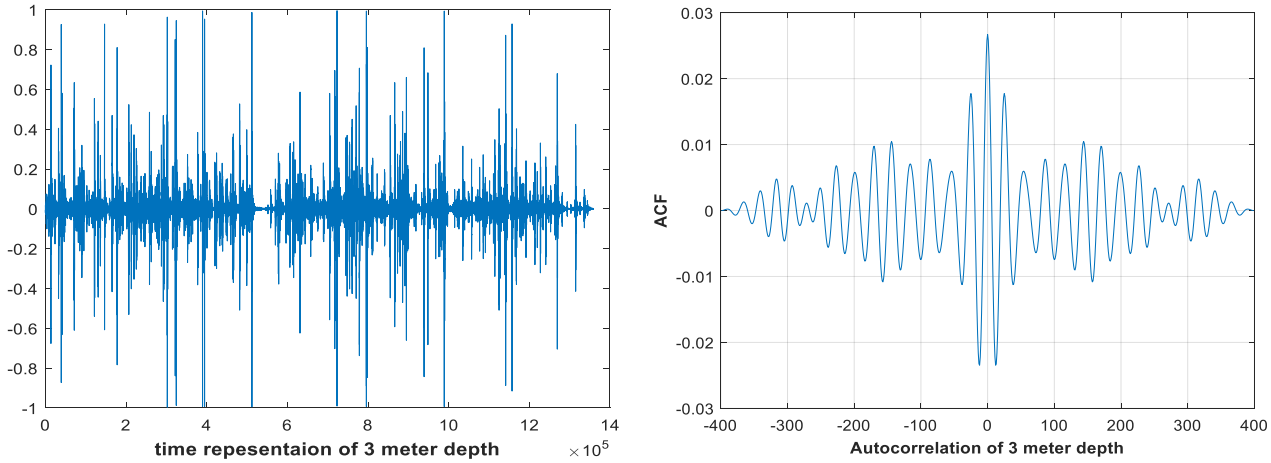

(b)

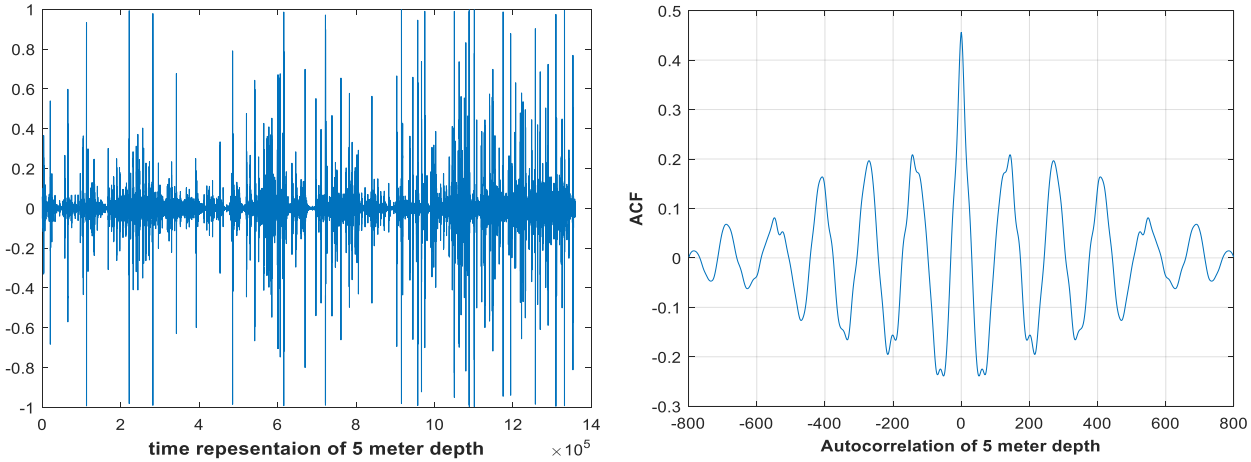

(c)

Figure 2. The ACF and signal waveform of UWAN at 3 separate depths: a) 1 m, b) 2 m, and c) 5 m [19].

3. De-noising Process in UWAN

3.1. Model of de-noising system

UWAN, being classified as a pink or simply colored noise, makes typical AWGN noise de-noising methods ineffective [6]. In contrast, employing a universal threshold estimation method to denoise this specific form of noise could provide greater advantages [12]. The signal is transformed into a time-frequency domain, which enables the application of the threshold at each level to remove the colored noise. The last stage is to use the new coefficients to rebuild the original signal. Fig. 3 illustrates the configuration for the de-noising signal system.

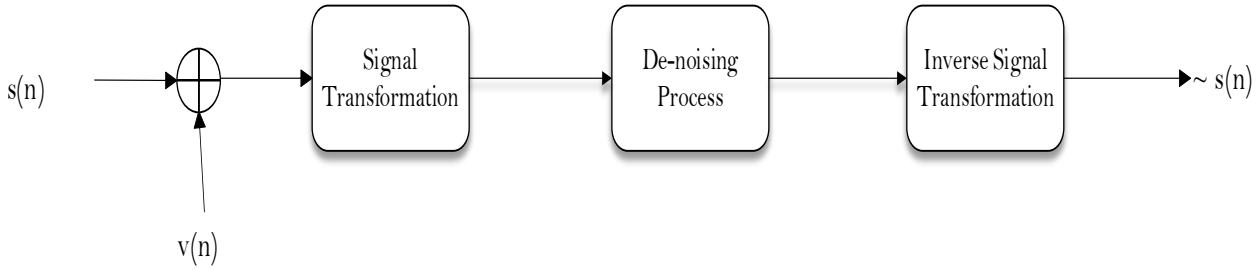

Figure 3. De-noising system.

3.2. Signal transforms

To do de-noising, the signal must be converted to a domain called time-frequency. This enables the application of a level-dependent threshold estimate for the colored UWAN. This work utilizes two techniques: the Discrete Wavelet Transform (DWT) and the enhanced Complex Wavelet Transform (CWT).

3.2.1. Wavelet transform.

An alternative to the Fourier Transform (FT) is the Wavelet Transform (WT), which employs small, localized waves called wavelets in place of an infinitely oscillating sinewave [12]. WT converts a signal to a representation of time and frequency. WT can be described as a continuous time or discrete time transform, just as the Fourier Transform. The formula for continuous WT (CoWT) is [10]:

$$X(a,\tau) = \frac{1}{\sqrt{a}} \int_{-\infty}^{\infty} x(t) * \psi\left(\frac{t-\tau}{a}\right) dt \quad (8)$$

The scale factor is a, the shift factor is τ, and $\psi_{a,b}$is the basis wavelet function, also called the mother function. Wavelets come in many different shapes, such as Biorthogonal, Debauchies, Symlet, and Coiflet [20]. The selection of the basis function is dependent upon the characteristics of the signal.

Since the signal is discrete, a more suitable method is the Discrete Wavelet Transform (DWT). The DWT can be mathematically represented as:

$$X(\tau,a) = \frac{1}{\sqrt{a}} \sum_{i=0}^{N-1} x(i)\, \psi\left(\frac{i-\tau}{a}\right) \quad (9)$$

The variable τ denotes the temporal shift, whereas the variable a reflects the magnitude of the scale. A discrete version of wavelet transform (WT) can be applied using a technique known as Filter bank design form. A filter bank utilizes low-pass and high-pass filters. [21]. The details Df and approximation Cf are the outputs and are down-sampled by 2 in these filters [21]. To achieve the desired degree of decomposition, the signal is subjected to L levels of these filters. Fig. 4, displays a DWT filter bank with three distinct levels.

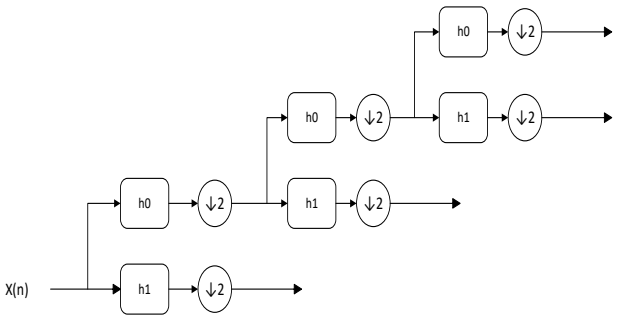

Figure 4. DWT filter bank with three levels [20].

3.2.2. Complex wavelets transform.

The Complex Wavelets Transform, also known as Dual-Tree Discrete Wavelet Transform (DT-DWT), is generated by using a set of wavelet trees that create a pair of Hilbert transforms [22]. The design features a set of trees, classified as both real and imaginary trees, which may be denoted as Tree A and Tree B [22]. Equation (10) illustrates the relationship between the wavelet functions in the two trees. For each real tree, let ψ_{re} represent its wavelet and ψ_{im} represent its imaginary wavelet [20]:

$$\psi_{im} = \mathrm{H}\{\psi_{re}\} = \begin{cases} -j\,\psi_{re} & \omega \geq 0 \\ j\,\psi_{re} & \omega < 0 \end{cases} \quad (10)$$

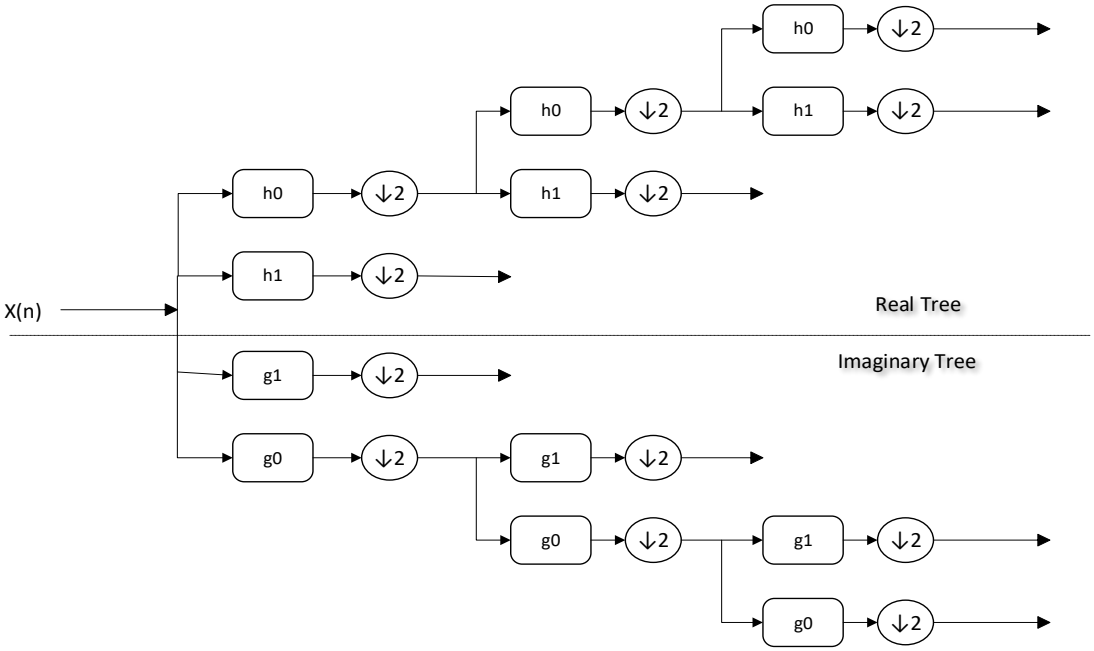

Figure 5. The Complex Wavelet Transform Analysis filter [20].

As previously noted, two trees are used to produce DT-DWT. The constructed filter, known as an analysis filter, had a low-pass filter in the real tree that would be delayed by half a sample compared to the same filter in the imagined tree [20]. A perfect signal reconstruction is achieved by implementing the Hilbert transform pair, which requires a specific delay [22]. In Fig. 5, the demonstration shows a common DT-DWT filter design with the real tree's low-pass and high-pass filters represented by e0 and e1, and the imaginary tree's equivalent filters by w0 and w1. The relationship between the imaginary tree's low-pass filters and those in the real tree is shown below [22]:

$$w0(n) = e0\left(n - \frac{1}{2}\right) \quad (11)$$

Equation (11) can be expressed in Fourier transform:

$$W0(\omega) = E0(\omega)\, e^{-j\theta(\omega)} \quad (12)$$

Where $\theta(\omega) = \frac{\omega}{2}$, $|\omega| < \pi$

The process of reconstructing the original signal follows a procedure similar to the standard wavelet, but with the difference that there will be two signals from the real and imaginary components. By computing the mean of signals, it's possible to precisely recover the original signal [17]. A synthesis filter refers to a filter bank that performs the reverse Complex wavelet transform [17]. Fig. 6, illustrates the synthesis filter used in the DT-DWT transform.

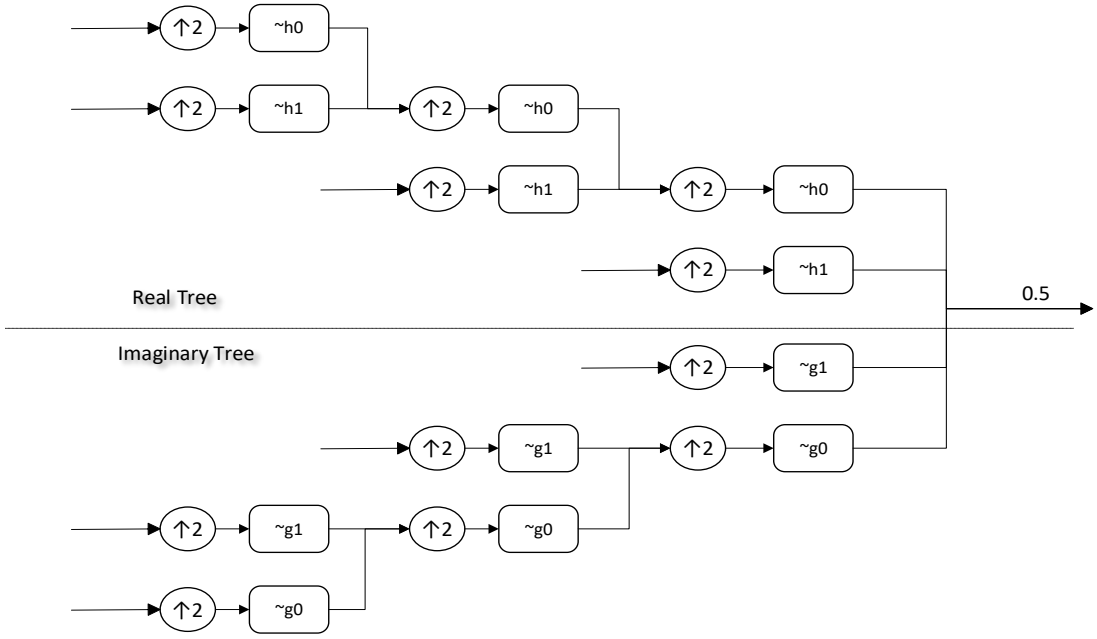

Figure 6. Complex wavelet transforms synthesizer filter [17]

3.3 De-noising approach

This section describes the de-noising techniques using the Wavelet transform and Complex Wavelet transform, as shown in Fig. 3.

3.3.1 Wavelet-based approach

The algorithm for de-noising in DWT, to restore the original signal s(n) that has been affected by noise v(n), has three steps:

- Decomposition: Select a suitable wavelet and specify a decomposition level L. Calculate the components of the signal that has noise at level L.
- Threshold: Find the detailed coefficients for each level and calculate their threshold values. A technique called Universal threshold estimation is used to calculate the threshold.
- Reconstruction: Using the new coefficients, execute an inverse wavelet transform to recover the source signal S(n).

The technique for executing the thresholding at the time-frequency domain with the Discrete Wavelet Transform (DWT) is explained in detail in reference [10]. The threshold for the kth level is determined using the modified Universal threshold estimate method [21]:

$$\lambda_k = c\ \sigma_k * \sqrt{2\log(N)} \quad (13)$$

The signal's length at level k is denoted as N, and the standard deviation for the noise at the kth level is denoted as σ_k, and the modified universal threshold parameter is denoted as c. The parameter has a value of $0 < c > 1$.

The expression for the standard deviation of the kth level is, let Y_D be details coefficients:

$$\sigma_k = \frac{median(|Y_D(n,k)|)}{0.6745} \quad (14)$$

When white noise exists in the channel, the standard deviation is calculated using the details coefficients of the first level. The reason for this is that the white noise evenly distributes power across all frequencies.

The original signal is obtained after the noise is eliminated using the calculated threshold. In [12], the factor c is added to maximize the de-noising efficiency. A step value of 0.1 is gradually applied to find the appropriate value of c. The relevant value of c is then determined by monitoring the output SNR.

Next, using a soft threshold approach [10], thresholding is done to the detail's coefficients $Y_D(n,k)$ at every level, as illustrated in (15):

$$Y_{D,\lambda}(n,k) = \begin{cases} sgn\big(Y_D(n,k)\big)(|Y_D(n,k)| - \lambda_k) if\ |Y_D(n,k)| > \lambda_k \\ 0 \qquad\qquad if\ |Y_D(n,k) \le \lambda_k \end{cases} \quad (15)$$

Soft thresholding involves setting any coefficients with magnitudes lower than or equal to the threshold value λ_k to zero and reducing any coefficients with a magnitude that is larger than the threshold by the threshold value. [12]. Another method of thresholding, referred to as hard thresholding, involves setting any coefficients with a magnitude less than or equal to the threshold level λ_k to zero while retaining the rest of the coefficients with their original values [12].

The reconstruction technique utilizes the new detail coefficients $Y_{D,\lambda}(n,k)$ and the approximation coefficients of level L, $Y_{A,L}(n,k)$, to restore the original signal (16). This method includes up-sampling by a factor of 2.

$$x(n) = Y_{A,L}(n,k) + \sum_{i=1}^{L} Y_{D,\lambda,i}(n,k) \quad (16)$$

3.3.2 Complex wavelet-based approach

The two trees in the DT-DWT operate in parallel offering the speed of DWT. However, this feature comes at the cost of memory requirements [17]. The signal x(n) is decomposed in DT-DWT using two filter banks, the output is the information from the real tree as well as its Hilbert-transform representation in the imaginary tree. Fig. 7, shows the utilized algorithm in the de-noising process. At the kth level, detailed coefficients could be expressed as:

$$Y_D(n,k) = Y_{D,re}(n,k) + jY_{D,im}(n,k) \quad (17)$$

Due to the existence of two trees, one real and one imaginary, the computation of the threshold value will be carried out independently for each tree at every level. The Real and Imaginary trees' threshold estimation is provided as:

$$\lambda_{k,re} = c\ \sigma_{k,re}\sqrt{2\log(N)}$$
$$\lambda_{k,im} = c\ \sigma_{k,im}\sqrt{2\log(N)} \quad (18)$$

Where the noise deviations for the imaginary and real trees are represented by the variables $\sigma_{k,im}$ and $\sigma_{k,}$ re. The following formula is used to get the level k standard deviations:

$$\sigma_{k,re} = \frac{median(|Y_{D,re}(n,k)|)}{0.6745}$$
$$\sigma_{k,im} = \frac{median(|Y_{D,im}(n,k)|)}{0.6745} \quad (19)$$

Once the threshold values have been determined, the next step will be to use the soft thresholding method as described below:

$$Y_{D,re,\lambda}(n,k) = \begin{cases} sgn\left(Y_{D,re}(n,k)\right)\left(|y_{D,re}(n,k)| - \lambda_{k,re}\right) if\ |Y_{D,re}(n,k)| > \lambda_{k,re} \\ 0 \qquad\qquad if\ |Y_{D,re}(n,k) \le \lambda_{k,re} \end{cases}$$

$$Y_{D,im,\lambda}(n,k) = \begin{cases} sgn\left(Y_{D,im}(n,k)\right)\left(|Y_{D,im}(n,k)| - \lambda_{k,im}\right) if\ |Y_{D,im}(n,k)| > \lambda_{k,im} \\ 0 \qquad\qquad if\ |Y_{D,im}(n,k) \le \lambda_{k,im} \end{cases} \quad (20)$$

The soft threshold approach is utilized to eliminate noise from the detail's coefficient of both the real and imaginary trees, therefore restoring the original signal. While hard thresholding is an alternative approach, soft thresholding demonstrates superior performance compared to hard thresholding by decreasing the sudden changes in the thresholded signal.

The reconstruction procedure is the final stage, in which the original is restored by utilizing the newly obtained detail coefficients. The synthesis or backward filter, as seen in Fig. 6, utilizes the time-reversed coefficients of the analysis filter [20],

used in the first stage. These coefficients correspond to the lowpass and high-pass filters. In a manner identical to the Discrete Wavelet Transform (DWT), the reconstruction process restores the signal. However, in this case, there will be two copies of the signal derived from both trees the real one and the imagined one. A reconstruction equation provided in (16) is going to be utilized to restore the signal from both trees. By calculating the mean of the two signals, the de-noised signal is achieved, as demonstrated:

$$x_{re}(n) = Y_{A,re,L}(n,k) + \sum_{i=1}^{L} Y_{D,re,\lambda,i}(n,k) \quad (21)$$

$$x_{im}(n) = Y_{A,im,L}(n,k) + \sum_{i=1}^{L} Y_{D,im,\lambda,i}(n,k) \quad (22)$$

$$x(n) = \frac{x_{re}(n)+x_{im}(n)}{2} \quad (23)$$

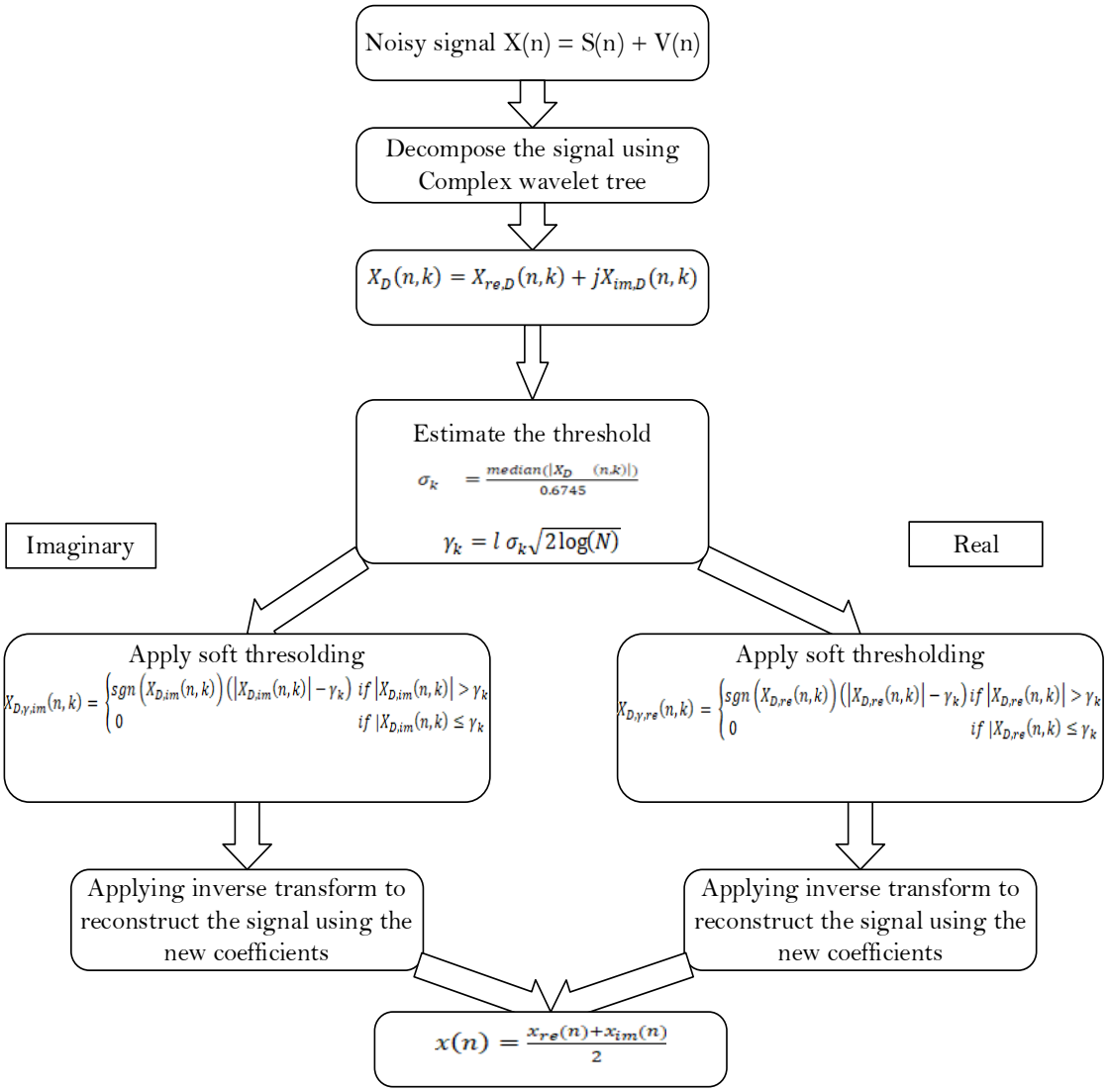

Figure 7. The complete DT-DWT proposed algorithm.

3.4 Performance measures

The performance of the various de-noising methods and the quality of the output signal are primarily assessed using two parameters: signal-to-noise ratio (SNR) as well as root mean squared error (RMSE) [16]. One definition of the SNR is:

$$SNR = 10\log\left[\frac{\sum_{n=1}^{N} s(n)^2}{\sum_{n=1}^{N}[\tilde{s}(n)-s(n)]^2}\right] \quad (24)$$

where N is the signal's length, $s(n)$ is the originally sent signal, and $\tilde{s}(n)$ is the signal following de-noising. If the output signal-to-noise ratio (SNR) exceeds the input SNR, the de-noising process is deemed effective.

One definition of the RMSE is:

$$RMSE = \sqrt{\frac{1}{N}\sum_{n=1}^{N}[\tilde{s}(n) - s(n)]^2} \quad (25)$$

The root-mean-squared error (RMSE) evaluates how closely the de-noised signal matches the original signal. Using these criteria, the suggested approach is evaluated and compared to DWT. The results of the optimal de-noising method show minimized RMSE and maximized SNR.

4. Results and Discussion.

The utilized techniques for signal de-noising are evaluated and simulated using a UWAN. The used UWAN is Tigers River real data [19]. The signals utilized in this evaluation are defined by (1 - 4). Here are the signals:

- A 100k-sample fixed-frequency signal with a 200 Hz.
- A 100k sample long LFM signal with a starting frequency of 10 Hz and a 500 Hz peak frequency.

8000 Hz is the sampling frequency used for the signals. With the noise power remaining constant, the simulation is run at SNR values between -2 and 6 dB by varying the signal amplitude. Measurements were collected at depths of 1m, 3m, and 5m and later utilized in simulation [19]. The decomposition level for both DWT and DT-DWT was set to 4. The DWT utilizes the Daubechies wavelet and soft thresholding technique [23]. The coefficients of DT-DWT are selected from [22] and the results are achieved by using soft thresholding.

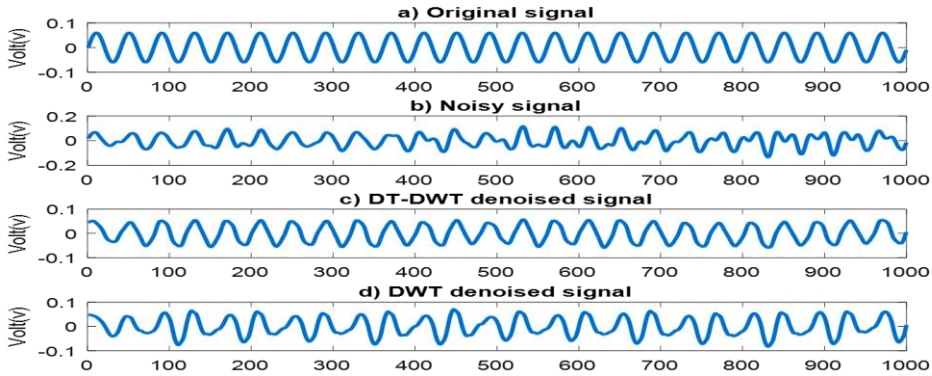

a) Fixed frequency signal with 200 Hz frequency

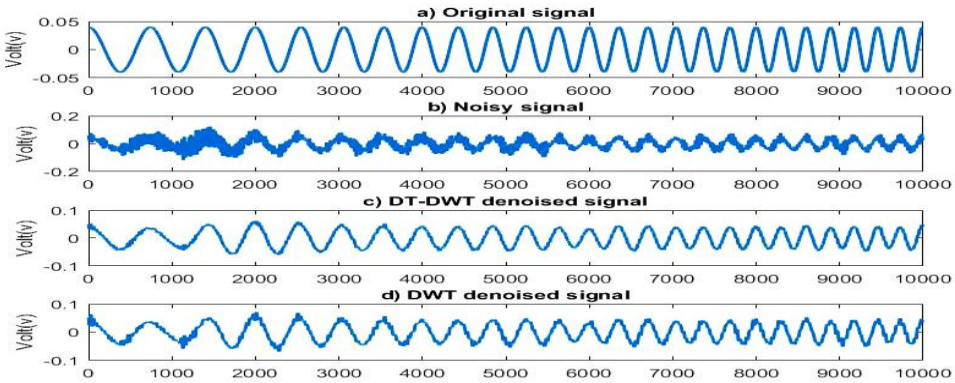

b) LFM signal

Figure 8. Four waves presented for 3 m depth: a) signal of interest, b) signal with noise, c) DT-DWT de-noised signal, and d) DWT de-noised signal [Input SNR -1.2].

Fig. 8, illustrates the time-domain representation of the signal of interest, signal with noise, and de-noised signals using various approaches. There is a noticeable difference in performance between the Discrete Wavelet Transform (DWT) and the Dual-Tree Complex Wavelet Transform (DT-DWT). Because UWAN's PSD depends on frequency, the power is concentrated in the low frequency, as seen in Fig. 8(b). Fig. 9, presents a comparison of the signal-to-noise ratio (SNR) outputs of several de-noising techniques at depths of 1 meter, 3 meters, and 5 meters. If the signal at the output has a signal-to-noise ratio (SNR) that is higher than the signal at the input, then the de-noising process is considered to have been successful.

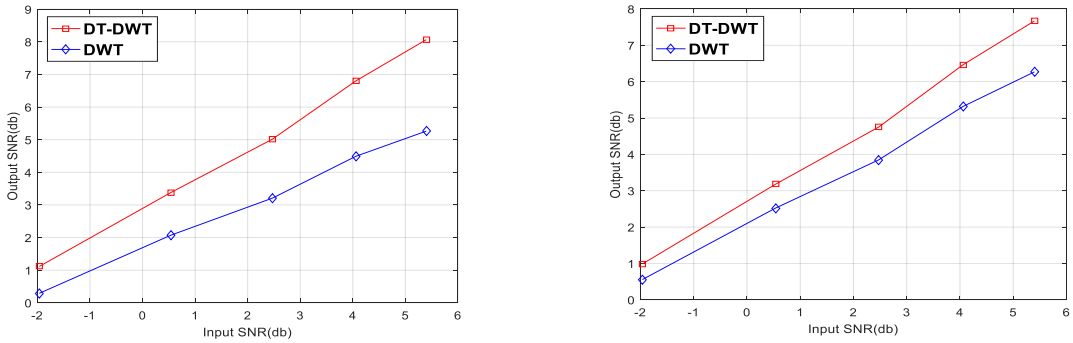

(a) (b)

i) 1m depth for a) 200 Hz fixed frequency and b) LFM signal.

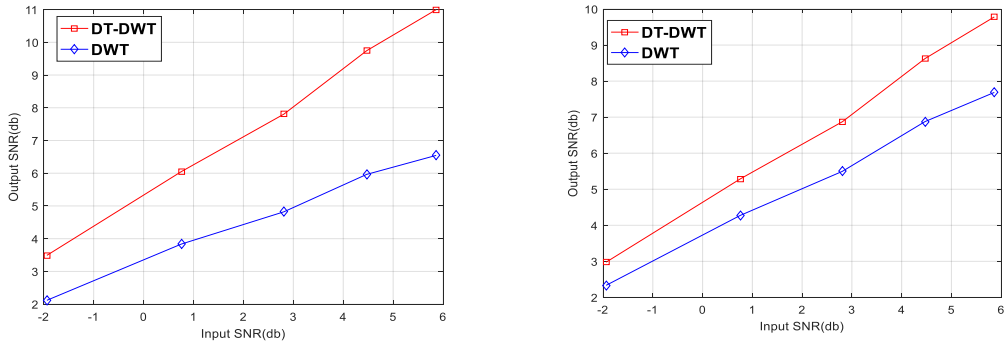

(a) (b)

ii) 3m depth for a) 200 Hz fixed frequency and b) LFM signal.

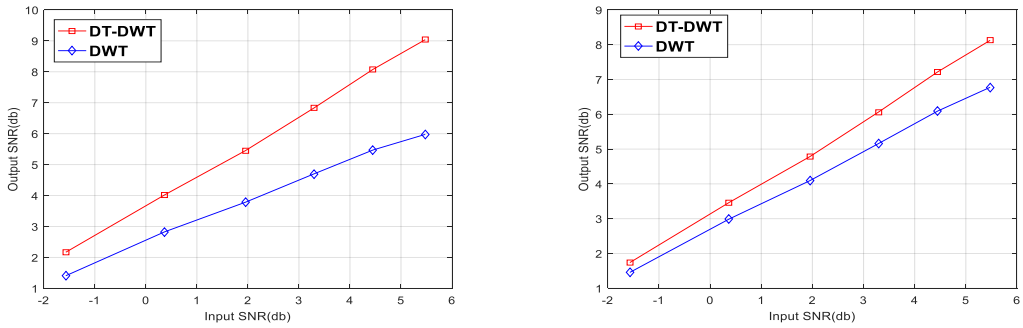

(a) (b)

iii) 5m depth for a) 200 Hz fixed frequency and b) LFM signal.

Figure 9. DWT and DT-DWT achieved SNR at 1m, 3m, and 5m depth.

As demonstrated before, the DT-DWT consistently outperforms the DWT in all scenarios. An SNR difference of around 3 dB was seen between the DT-DWT and DWT approaches at a depth of 1m, with an input SNR of 5.5 dB. This difference was recorded for a constant frequency. In the case of an LFM signal, the observed difference was 2 dB.

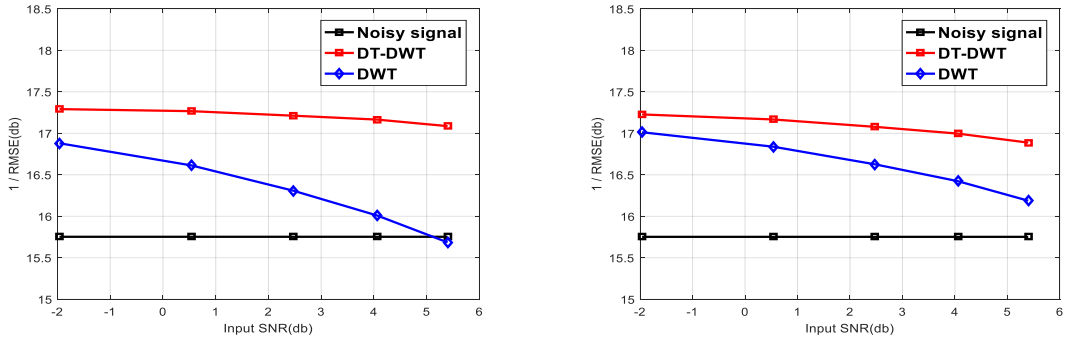

(a) (b)

i) 1m depth for a) 200 Hz fixed frequency and b) LFM signal.

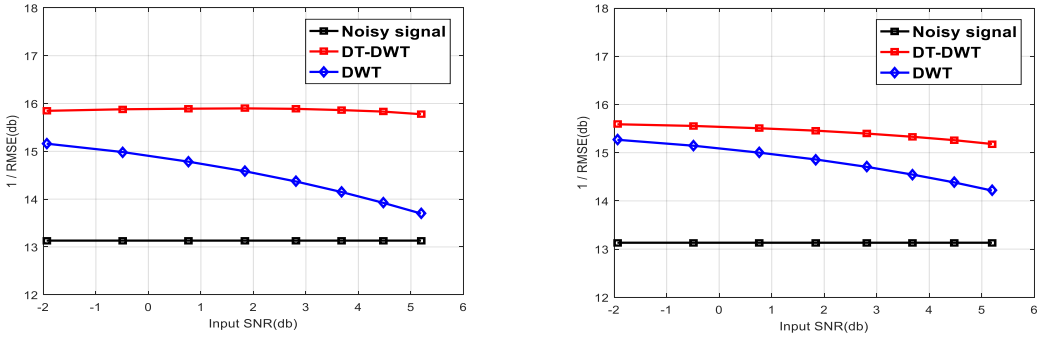

(a) (b)

ii) 1m depth for a) 200 Hz fixed frequency and b) LFM signal.

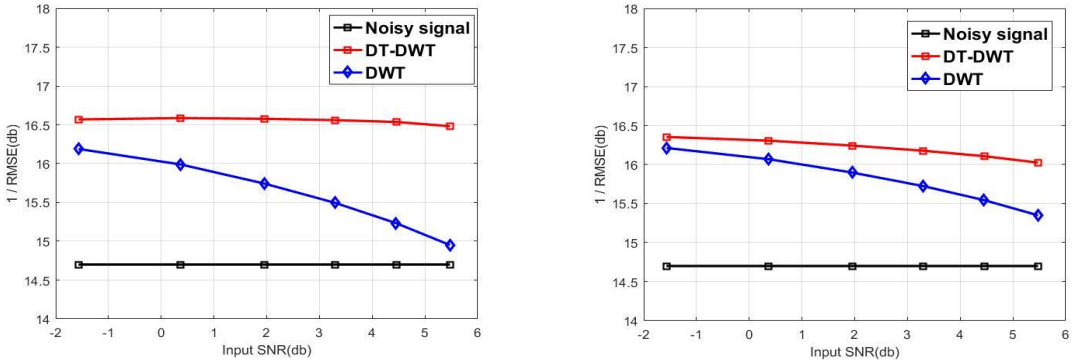

(a) (b)

iii) 5m depth for a) 200 Hz fixed frequency and b) LFM signal.

Figure 10. The obtained RMSE values at 1 m, 3 m, and 5 m using DWT and DT-DWT.

Fig. 10, displays the comparison of RMSE values at different depths when the input SNR varied from -2 dB to 6 dB. In all circumstances, the DT-DWT de-noising approach consistently exhibits reduced error compared to the DWT de-noising approach. When comparing the two techniques of reducing noise at a depth of 3 meters, there was an observed difference of approximately 2 dB for the fixed frequency approach and roughly 3 dB for the LFM signal method, with an input signal-to-noise ratio of 5.5 dB.

Table 1 shows the SNR and RMSE values for the two de-noising techniques. The results obtained are founded on a fixed input SNR of 5.9 dB and a 3-meter-deep input RMSE of -13.2 dB.

Table 1. Various de-noising algorithms output RMSE and SNR for 5.9 dB input SNR and -13.2 dB input RMSE at 3m depth.

Measures	**DWT**	**DT-DWT**
Fixed frequency at 200 Hz		
Output SNR (dB)	6.5	10.9
1/RMSE (dB)	13.5	15.7
LFM signal		
Output SNR (dB)	7.6	9.7
1/RMSE (dB)	14.05	15.09

5. Conclusion

this paper investigates the performance of the time-frequency techniques for de-noising an acoustic signal in actual UWAN data that was recorded and is known to contain colored noise. To do this, the DT-DWT method was utilized to create a representation of the signal in the time-frequency domain. After that, a de-noising technique using a threshold that varies depending on the decomposition level of the signal was applied. Modified universal threshold estimate is the method used to figure out the threshold at each level. The performance of DT-DWT was compared with the commonly used DWT. For testing and simulating the de-noising algorithms, real-world noise data was added to two types of signals: LFM and fixed-frequency signals. The two signals are utilized in the simulation. The results indicated that DT-DWT has a better performance compared to DWT, demonstrating its higher efficiency. The result of the fixed frequency signal and LFM signal, respectively, there was a 2dB and a 3dB difference in SNR between the two denoising techniques.

Conflict of interest

The authors declare that there are no conflicts of interest regarding the publication of this manuscript.

Author Contribution Statement

This document was written and edited in part by each Author. The study topic was suggested and the results of this work were supervised by the authors, Yasin Al-Aboosi, and Nor Shahida Mohd Shah. The manuscript structure was prepared by author Ausama Khalid. Each author contributed to the final text and discussed the findings.

References

[1]. K. M. Awan et al., "Underwater Wireless Sensor Networks: A review of recent issues and challenges," *Wireless Communications and Mobile Computing*, vol. 2019, pp. 1–20, Jan. 2019. https://doi.org/10.1155/2019/6470359

[2]. S. Mangione, G. E. Galioto, D. Croce, I. Tinnirello, and C. Petrioli, "A Channel-Aware adaptive modem for underwater acoustic communications," *IEEE Access*, vol. 9, pp. 76340–76353, Jan. 2021, https://doi.org/10.1109/access.2021.3082766.

[3]. D. H. Muhsen, A. B. Ghazali, T. Khatib, and I. A. Abed, "Extraction of Photovoltaic Module Model's Parameters Using an Improved Hybrid Differential evolution/electromagnetism-like Algorithm," Solar Energy, vol. 119, pp. 286–297, Sep. 2015, https://doi.org/10.1016/j.solener.2015.07.008.

[4]. K. Y. Islam, I. Ahmad, D. Habibi, and A. Waqar, "A survey on energy efficiency in underwater wireless communications," *Journal of Network and Computer Applications*, vol. 198, p. 103295, Feb. 2022, https://doi.org/10.1016/j.jnca.2021.103295.

[5]. A. Monczak, C. Mueller, M. Miller, Y. Ji, S. Borgianini, and E. Montie, "Sound patterns of snapping shrimp, fish, and dolphins in an estuarine soundscape of the southeastern USA," *Marine Ecology Progress Series*, vol. 609, pp. 49–68, Jan. 2019, https://doi.org/10.3354/meps12813.

[6]. C. W. Therrien, *Discrete random signals and statistical signal processing*. 1992. [Online]. Available: https://ci.nii.ac.jp/ncid/BA20809722.

[7]. L.-M. Dogariu, J. Benesty, C. Paleologu, and S. Ciochină, "An insightful overview of the Wiener filter for system identification," *Applied Sciences*, vol. 11, no. 17, p. 7774, Aug. 2021, https://doi.org/10.3390/app11177774.

[8]. S. Bharati, T. Z. Khan, P. Podder, and N. Q. Hung, "A Comparative Analysis of Image Denoising Problem: Noise models, Denoising Filters and Applications," in *Studies in Systems, Decision and Control*, 2020, pp. 49–66. https://doi.org/10.1007/978-3-030-55833-8_3.

[9]. L. Xu, S. Chatterton, and P. Pennacchi, "Rolling element bearing diagnosis based on singular value decomposition and composite squared envelope spectrum," *Mechanical Systems and Signal Processing*, vol. 148, p. 107174, Feb. 2021, https://doi.org/10.1016/j.ymssp.2020.107174.

[10]. D. L. Donoho and I. M. Johnstone, "Ideal spatial adaptation by wavelet shrinkage," *Biometrika*, vol. 81, no. 3, pp. 425–455, Sep. 1994, https://doi.org/10.1093/biomet/81.3.425

[11]. Y. Xu, J. B. Weaver, D. M. Healy, and J. Lu, "Wavelet transform domain filters: a spatially selective noise filtration technique," *IEEE Transactions on Image Processing*, vol. 3, no. 6, pp. 747–758, Jan. 1994, https://doi.org/10.1109/83.336245

[12]. R. Aggarwal, J. K. Singh, V. K. Gupta, S. Rathore, M. Tiwari, and A. Khare, "Noise Reduction of Speech Signal using Wavelet Transform with Modified Universal Threshold," *International Journal of Computer Applications*, vol. 20, no. 5, pp. 14–19, Apr. 2011, https://doi.org/10.5120/2431-3269

[13]. A. Z. Sha'ameri, Y. Y. Al-Aboosi, and N. H. H. Khamis, "Underwater acoustic noise characteristics of shallow water in tropical seas,". *Proc. Of the International Conference on Computer & Communication Engineering 2014 (ICCCE 2014)*, Sep. 2014, https://doi.org/10.1109/iccce.2014.34

[14]. T. E. Murad and Y. Al-Aboosi, "Bit Error Performance Enhancement for Underwater Acoustic Noise Channel by Using Channel Coding," *Journal of Engineering and Sustainable Development*, vol. 27, no. 5, pp. 659–670, Sep. 2023, https://doi.org/10.31272/jeasd.27.5.8

[15]. M. S. Mahmood and Y. Y. Al-Aboosi, "Effects of Multipath Propagation Channel in Tigris River," *Journal of Engineering and Sustainable Development*, vol. 27, no. 2, pp. 256–271, Mar. 2023, https://doi.org/10.31272/jeasd.27.2.9

[16]. Y. Y. Al-Aboosi, M. S. Ahmed, and A. A. Sahrab, "Near–Optimum Detection of Signals in Underwater Acoustic Noise Using Locally Optimal Detector in Tigers River," *Journal of Engineering and Sustainable Development*, vol. 27, no. 1, pp. 19–27, Jan. 2023, doi: https://doi.org/10.31272/jeasd.27.1.2

[17]. I. W. Selesnick, R. G. Baraniuk, and N. C. Kingsbury, "The dual-tree complex wavelet transforms," *IEEE Signal Processing Magazine*, vol. 22, no. 6, pp. 123–151, Nov. 2005, https://doi.org/10.1109/msp.2005.1550194

[18]. J. Panaro, F. Lopes, L. Barreira, and F. Souza, "Underwater acoustic noise model for shallow water communications," *Anais De XXX Simpósio Brasileiro De Telecomunicações*, Jan. 2012, https://doi.org/10.14209/sbrt.2012.85.

[19]. Mahmood, S. M., "Modeling and Performance Analysis of an Underwater Acoustic Communication Channel Using Ray Model" M.S. thesis, Dept. Electric Eng., Mustansiriyah Univ., Baghdad, Iraq, 2021.

[20]. SHUKLA, P., "Complex wavelet transforms and their applications" Ph.D. dissertation, Strathclyde Univ., Scotland, United Kingdom, 2003.

[21]. B. Dong, Q. Jiang, and Z. Shen, "Image restoration: Wavelet frame shrinkage, Nonlinear Evolution PDES, and beyond," *Multiscale Modeling & Simulation*, vol. 15, no. 1, pp. 606–660, Jan. 2017, https://doi.org/10.1137/15m1037457

[22]. I. W. Selesnick, "Hilbert transform pairs of wavelet bases," *IEEE Signal Processing Letters*, vol. 8, no. 6, pp. 170–173, Jun. 2001, doi: https://doi.org/10.1109/97.923042

[23]. A. Achmamad and A. Jbari, "A comparative study of wavelet families for electromyography signal classification based on discrete wavelet transform," *Bulletin of Electrical Engineering and Informatics*, vol. 9, no. 4, pp. 1420–1429, Aug. 2020, https://doi.org/10.11591/eei.v9i4.2381.